

Article

Geochemistry and Zircon U–Pb Geochronology of the Wugongshan Granites in the Northwestern Jiangxi Area, China: Implications for the Paleozoic Tectonic Development of South China

Guangqin Yang^{1,2}, Yaoyao Zhang^{1,*} , Kai Liu¹, Yi Zhou², Shuxun Wang^{1,2} and Hailong Huo^{2,*}

¹ Chinese Academy of Geological Sciences, Beijing 100037, China; yangguangqin88@163.com (G.Y.); acancer@163.com (K.L.); shux1999@163.com (S.W.)

² School of Gemmology, China University of Geosciences, Beijing 100083, China; zhoyi@cugb.edu.cn

* Correspondence: zhangyy@cags.ac.cn (Y.Z.); huohailong2012@163.com (H.H.)

Abstract: The properties of the Caledonian orogeny along the transition belt of the Yangtze and Cathaysia blocks have received much attention in recent years. The widespread Early Paleozoic granites provide critical geological clues for unraveling the tectonic evolution and geodynamic processes of the South China Continent (SCC). Here we present new zircon U–Pb chronology, whole-rock major and trace elements, in situ Hf isotopes for Paleozoic granites, i.e., the Wugongshan granites in the northwest Jiangxi province, and aim to explore the magmatism and properties of the Caledonian orogeny involved in their formation. Our new data show that the Wugongshan granites were emplaced during the Early Silurian Period (442–438 Ma). The Paleozoic Wugongshan granites belong to S-type muscovite-bearing peraluminous granites (MPG) and show a single origin. The Wugongshan granites exhibit negative $\epsilon_{\text{Hf}}(t)$ values (–11.56 to –6.19) and TDM2 model ages of 2148–1809 Ma, indicating their derivation from an ancient crustal source, through partial melting of ancient crustal material. The Wugongshan granitic magmatism is probably being generated in an extensional environment related to an intracontinental orogeny setting. It is inferred that the Paleozoic tectonic–magmatic event in the Wugongshan area was associated with the oceanic–continental convergence of the Paleo-Tethys Ocean. The Wugongshan granites highlight the intracontinental magmatism in the Early Paleozoic orogeny in the SCC.

Keywords: peraluminous S-type granite; intracontinental orogeny; Paleozoic; Wugongshan area; South China



Citation: Yang, G.; Zhang, Y.; Liu, K.; Zhou, Y.; Wang, S.; Huo, H. Geochemistry and Zircon U–Pb Geochronology of the Wugongshan Granites in the Northwestern Jiangxi Area, China: Implications for the Paleozoic Tectonic Development of South China. *Minerals* **2023**, *13*, 1427. <https://doi.org/10.3390/min13111427>

Academic Editors: Fuhao Xiong, Bin Liu and Michel Villeneuve

Received: 18 September 2023

Revised: 29 October 2023

Accepted: 1 November 2023

Published: 9 November 2023



Copyright: © 2023 by the authors. Licensee MDPI, Basel, Switzerland. This article is an open access article distributed under the terms and conditions of the Creative Commons Attribution (CC BY) license (<https://creativecommons.org/licenses/by/4.0/>).

1. Introduction

The South China Continent (SCC) is formed by the Yangtze block to the north and the Cathaysia block to the south, and finally collision along the Jiangshan–Shaoxing fault zone during the Meso-Neoproterozoic, and accompanied by the NE-trending Jiangnan orogenic belt (also known as the Jiangnan archicontinent, ca. 850–820 Ma), respectively (Figure 1a) [1–12]. Since the Neoproterozoic, South China has long been located in the global supercontinental convergence tectonic background, and experienced Neoproterozoic rifting (ca. 810–760 Ma), Caledonian orogeny (ca. 450–420 Ma), Indosinian intracontinental reworking (ca. 240–220 Ma) and Yanshanian intracontinental orogeny (ca. 180–145 Ma), which have formed the unique geological geomorphology of South China today [7,8,12–17]. Therefore, the tectonic properties of South China and the tectonic processes at different stages are of crucial significance for the reconstruction of global supercontinents [14,15,17–22].

For decades, a variety of geological studies have been performed in the SCC to understand its tectonic and magmatic evolution [13–15,23–26]. However, the Caledonian orogenesis of the SCC remains enigmatic [10,14,17,19,20,25–28]. The types of Caledonian

orogeny in South China are related to continental collision orogenies [10], or dominated by intracontinental orogenies [13,14,23,27,29], which need to be further studied [30,31]. The purpose of our study on the Wugongshan granites is to determine its petrogenesis and provide insights into the tectonic properties of the Caledonian orogeny in the SCC.

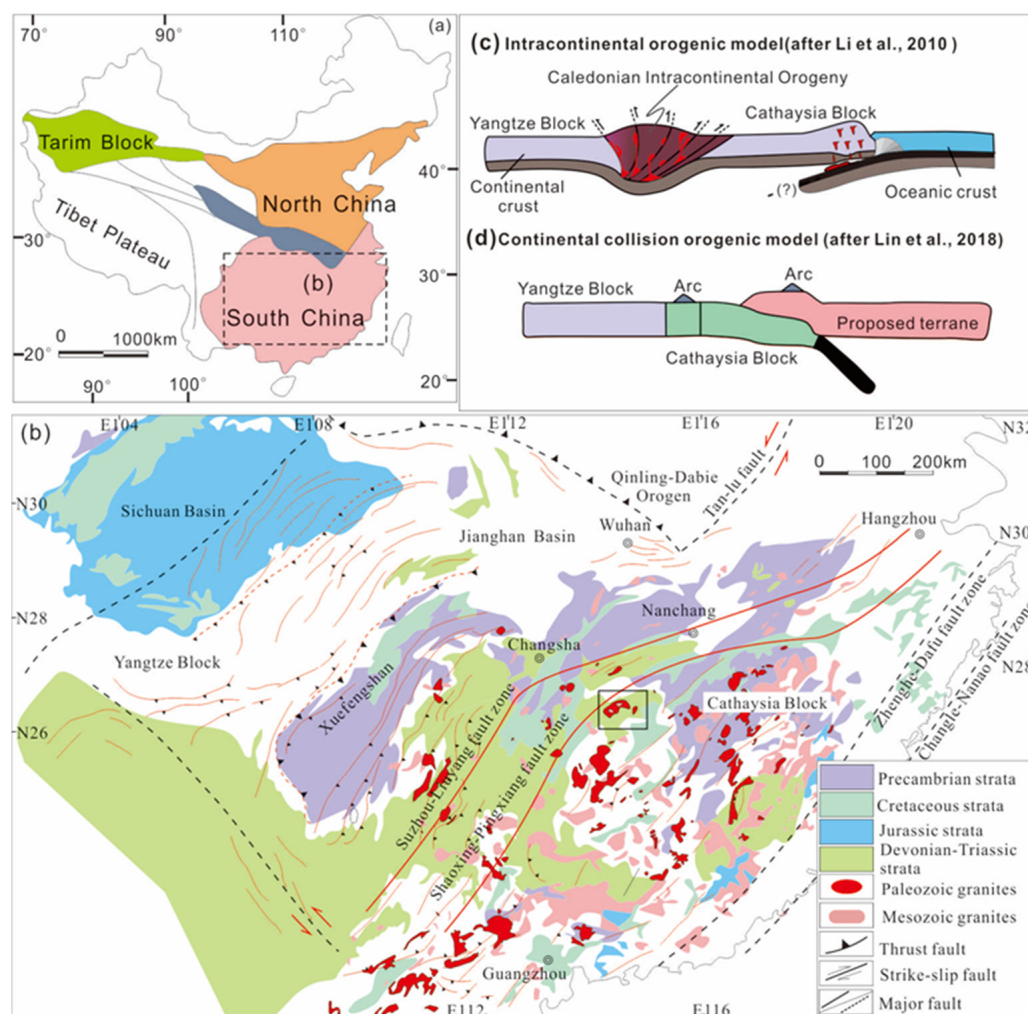


Figure 1. Geological map of Wugongshan area of the SCC. (a) The inset shows the location of the SCC, modified from [22]. (b) Sketch tectonic map of the Wugongshan and adjacent areas, modified from [31]. (c) Intracontinental orogenic model, modified from [14]. (d) Continental collision orogenic model, modified from [10].

The Wugongshan area is located on the northern edge of the Cathaysia block, on the western part of the Jiangshan–Shaoying fault zone (JSF). The Paleozoic magmatism is widely developed in the area and records complete information regarding the Paleozoic evolution of the SCC [16,20,24]. As an important junction of the Yangtze and Cathaysia blocks, the Wugongshan area provides a window to understanding the orogeny’s geological framework and the tectonic properties of the SCC during the Caledonian Period [3,13,14,19,32] (Figure 1b). For decades, previous studies have been made on the geological characteristics [33–35], petrology, geochemistry [36–41], and tectonic evolution [3,32] of the Early Paleozoic granite of the Wugongshan area. Although these studies provide insights into the Paleozoic granite’s evolution in the Wugongshan area, there has been no systematic analysis of the Caledonian tecto-magmatic evolutionary process of South China.

In this paper, we present zircon LA-ICP-MS U–Pb geochronological ages, in situ Hf isotopic data, and whole-rock major- and trace-element data for granites of the Wugongshan area. These new data, in conjunction with published data, help to constrain the relationships between Paleozoic orogeny and magmatic coupling process, and provide additional information concerning the Paleozoic tectonic evolution of South China.

2. Geological Setting

The basement strata in the Wugongshan area are Neoproterozoic–Cambrian weakly metamorphosed sandstone, uncomfortably overlain by the Devonian, Carboniferous–Triassic, and Quaternary strata [3,24,32,33,37,38] (Figure 2). The major lithologies of the Neoproterozoic–Cambrian are meta-greywackes, meta-volcanics, and phyllites, comprising a shallow-water, clastic-dominated meta-sedimentary environment [3,24,32].

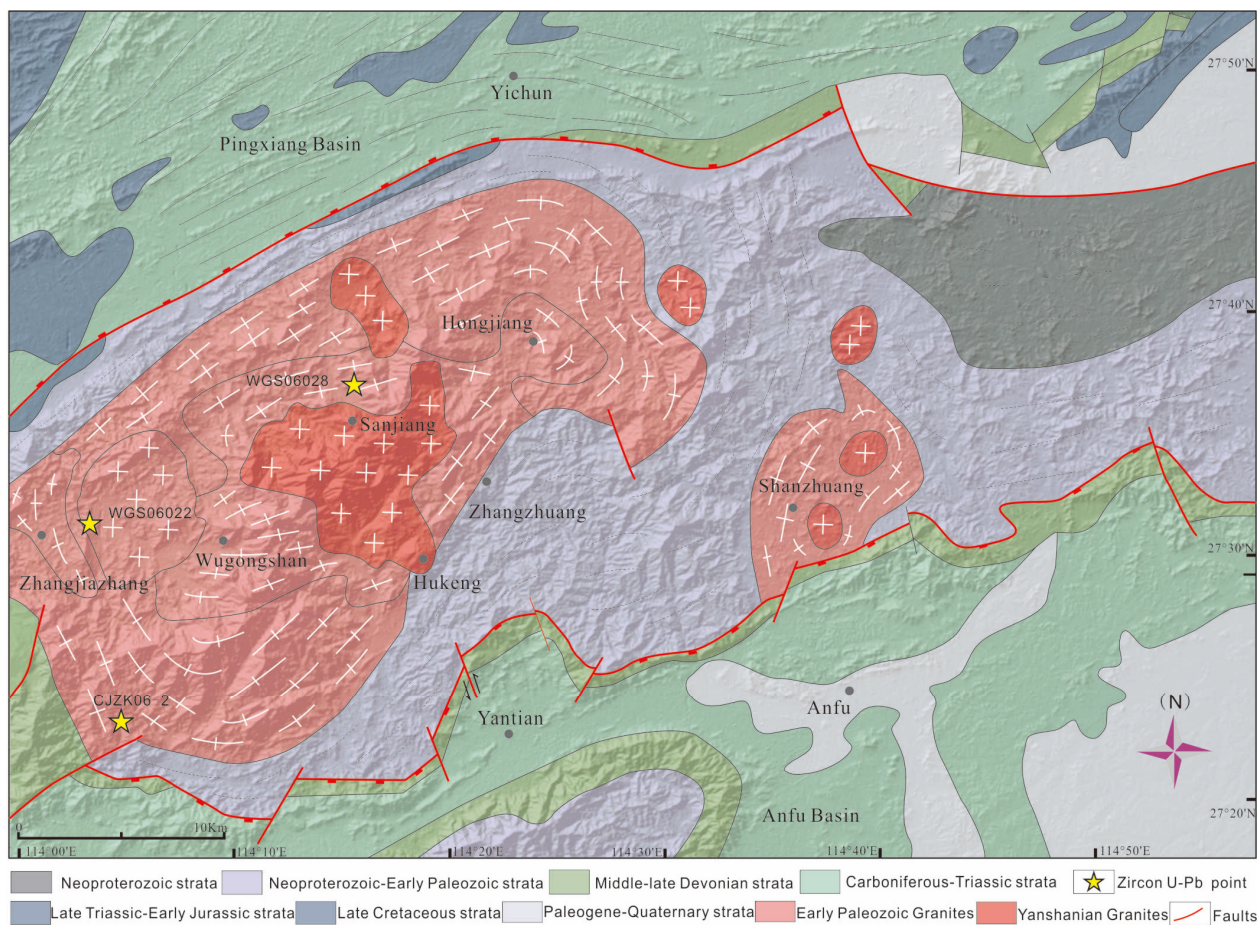


Figure 2. Simplified structural map of the Wugongshan area (modified from [3,32]).

The Anfu and Pingxiang basins have developed north and south of the Wugongshan granites (Figure 2). The granites are widely distributed in the Wugongshan area, with most being formed during the Early Paleozoic (Caledonian) and late Mesozoic (Yanshanian) [24,41]. The main rock types include porphyritic granite, gneissic granite, granodiorite biotite granite, two-mica granite, and muscovite granite. The Wugongshan pluton intruded into the Sinian and Cambrian meta-sedimentary strata, and the Yanshanian part consists of foliated gneiss granites in the Sanjiang and Qinglongshan, etc. [3,24,32,37,41].

3. Analytical Methods

In the present study, samples were collected from Xingqun, Qianshan, and Wanlongshan for detailed LA-ICP-MS U–Pb zircon age study, in situ Hf isotopic analyses, and geochemical analyses, with samples collected from different parts of the Wugongshan Paleozoic granites (Figure 2). The recent research shows that the geochemical elements change markedly along strong strain bands and siliceous veins in mylonitic granites, while the change in the geochemical characteristics away from strong strain bands can be ignored [42,43]. Therefore, in this study, to minimize the change in the geochemical characteristics of rocks by mylonitization, we selected samples far from the ductile shear zone, where mylonitization was weak and siliceous veins were absent.

3.1. LA-ICP-MS U–Pb and Hf Zircon Isotopic Analyses

Three representative fresh samples from the surface outcrop of the Wugongshan Paleozoic granites were selected for zircon LA-ICP-MS U–Pb analyses and in situ Hf isotopic dating. Zircon grains were extracted from the samples labeled CJK06–2, WGS06022, and WGS06022, using standard density and magnetic separation techniques, at the Hebei Institute of the Regional Geological Survey, Langfang City, Hebei Province, China. Zircons were photographed in reflected and transmitted light. Cathodoluminescence (CL) photographs of the zircons, LA-ICP-MS U–Pb zircon analyses, and in situ Hf isotopic dating were produced at Gaonian Linghang Technology LLC., Beijing, China, and the sites for zircon U–Pb and Hf analysis were based on these. The zircon U–Pb data and in situ Hf isotopic analyses were carried out using a Finnigan Neptune type LA-ICP-MS instrument with a New Wave UP213 laser, using laser-ablation spots of 20–30 µm diameter. 91,500 zircon and NIST 610 glass standards were used for calibration. Data processing was undertaken using Ludwig SQUID 1.03 and ISOPLOT 3.0 software [44–47]. Standard zircon Plešovice (337 ± 0.37 Ma) was used for quality control purposes during the in situ Hf isotopic analyses, and a weighted mean $^{176}\text{Hf}/^{177}\text{Hf}$ ratio of 0.282480 ± 0.000050 (2σ , $n = 18$), consistent with a published value of 0.282008 ± 0.000012 was used [48–50]. The results are listed in Supplementary Table S1.

3.2. Major- and Trace-Element Analyses

The major- and trace-element composition analyses were determined at the Hebei Institute of the Regional Geological Survey, Langfang City, Hebei Province, China. Major elements were identified using a Philips X-ray fluorescence spectrometer (XRF; Axiosmax). Analytical precision was better than ±5%. Trace elements were analyzed using a ThermoFisher X Series 2 (ICP-MS), using procedures similar to the [51]. The results are listed in Supplementary Tables S2 and S3.

4. Results

4.1. Petrography

We collected and analyzed the Early Paleozoic granites from different locations in Wugongshan granites. The representative lithologies included biotite monzonitic granite, two-mica monzonitic granite, and porphyritic two-mica monzonitic granite (Figure 3), which had different degrees of mylonitic characteristics, which are described as follows:

Biotite monzonitic granite (CJK06–2): It is grey in color, has a granitic texture and a mineral plagioclase (0.4–3.0 mm; 45%), K-feldspar (2–5 mm; 15%–20%), quartz (0.05–1.0 mm; 20%–25%), biotite (5%–10%), and minor muscovite (1%) content.

Two-mica monzonite granite (WGS06022): It is grey and composed of plagioclase (0.05–2.0 mm; 30%–45%), K-feldspar (0.05–2.0 mm; 30%–35%), quartz (0.1–3.0 mm; 25%), biotite and muscovite (total 10%). It has a granitic texture and displays a foliation defined by oriented biotite and muscovite.

Porphyritic two-mica monzonite granite (WGS06028): It is grey, has a granitic texture, and is composed of plagioclase (0.2–1.8 mm; 35%–40%), K-feldspar (2–9 mm; 30%–35%), quartz (0.1–0.7 mm; 20%–25%), biotite and muscovite (total 5%–10%).

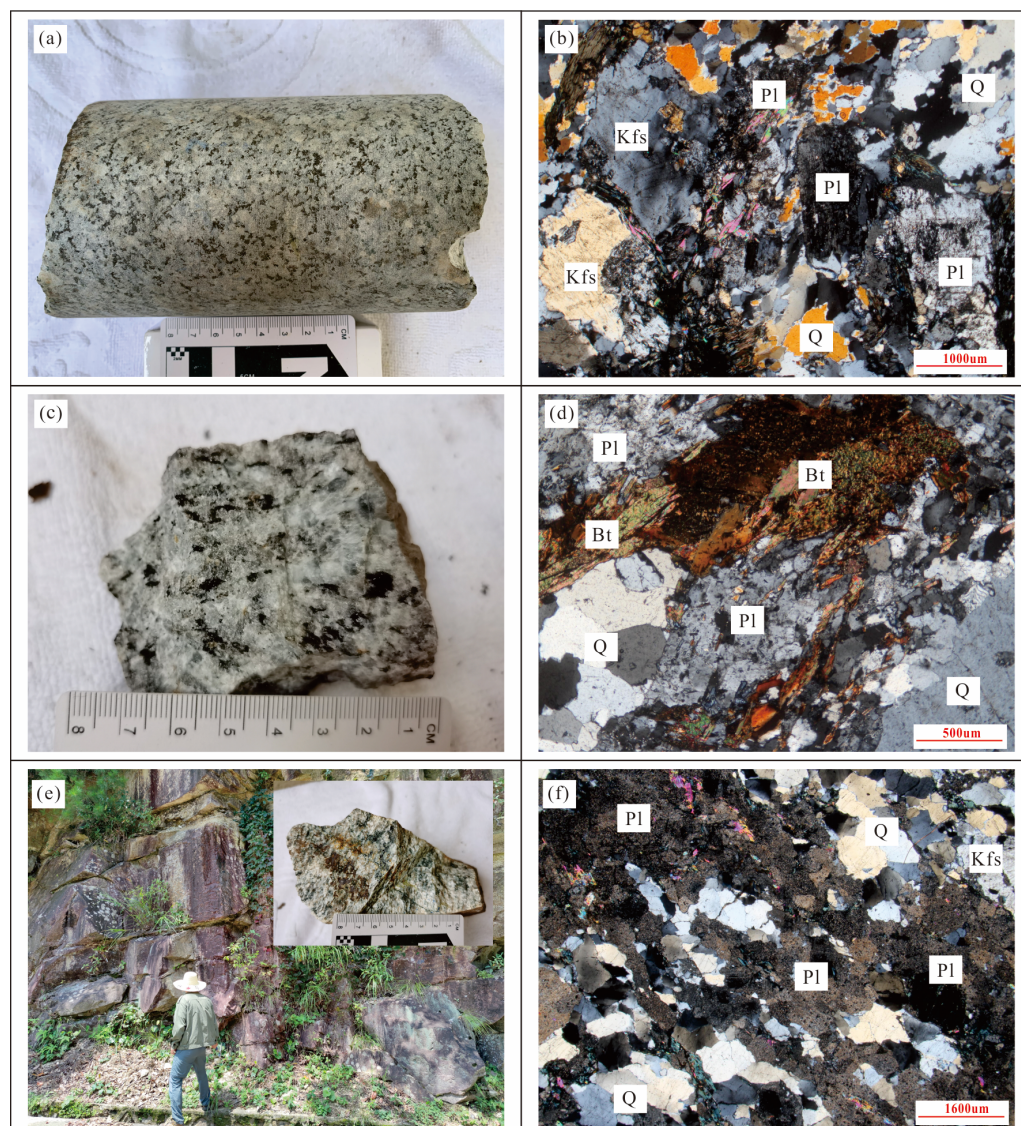


Figure 3. Field photographs and photomicrographs (crossed polar) of granites in the Wugongshan area: (a,b) biotite monzonitic granite; (c,d) two-mica monzonite granite; (e,f) porphyritic two-mica monzonite granite. Abbreviations: Q—quartz; Bt—biotite; Pl—plagioclase; Kfs—K-feldspar.

4.2. Geochronology and Hf Isotopic Compositions

Representative biotite monzonitic granite (CJK06–2), two-mica monzonite granite (WGS06022), and porphyritic two-mica monzonite granite (WGS06028) samples were collected for zircon U–Pb dating. Separated zircons are transparent, mostly euhedral or sub-rounded, and exhibit strong oscillatory zoning and high Th/U ratios (0.19–1.08), typical of a magmatic origin [52,53]. The analytical results for U–Pb and in situ Lu–Hf compositions are listed in Supplementary Tables S1 and S4.

Zircons with oscillatory zoning from samples CJK06–2, WGS06022, and WGS06028 were selected for $^{206}\text{Pb}/^{238}\text{U}$ dating (Figure 4). For sample CJK06–2, 26 zircon grains produced concordant results (within error), with a weighted-mean age of 438.9 ± 1.2 Ma (MSWD = 0.33) (Figure 4a). There were 27 analyses of WGS06022, which yielded a weighted-mean age of 439.4 ± 1.9 Ma (MSWD = 0.34) (Figure 4b). There were 31 analyses of WGS06028, which yielded a weighted-mean age of 441.9 ± 1.6 Ma (MSWD = 0.85) (Figure 4c).

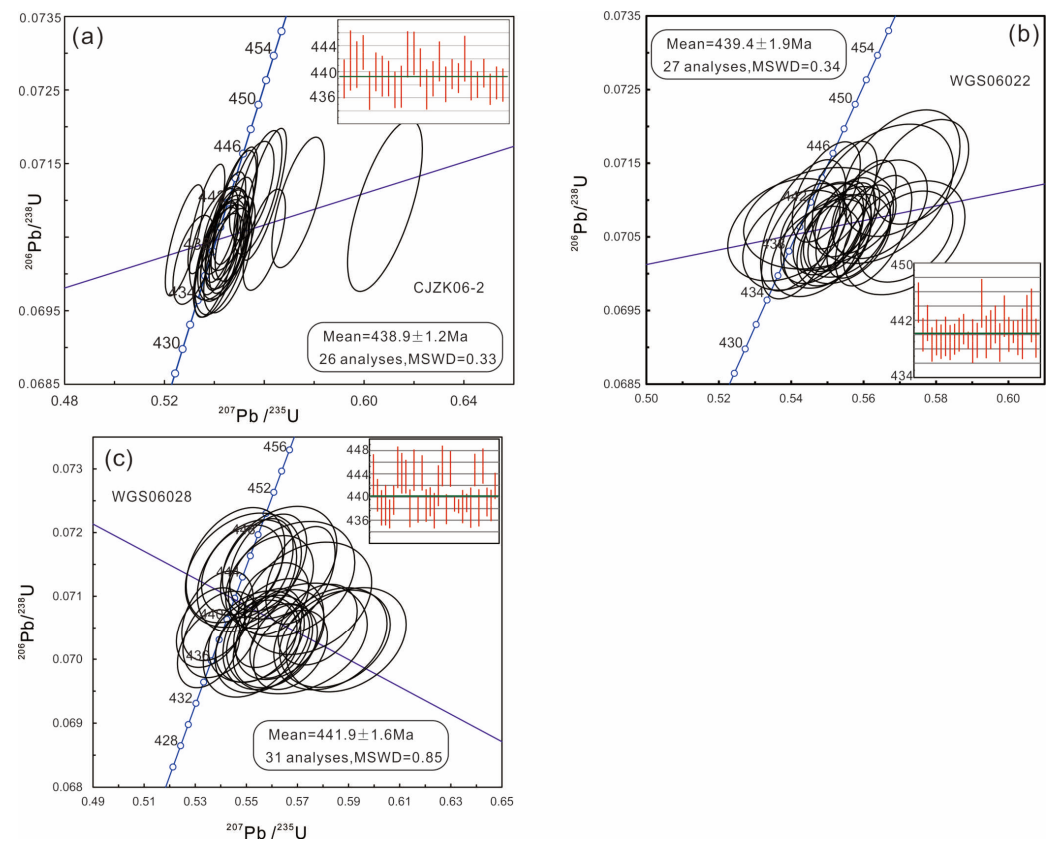


Figure 4. U–Pb concordia diagram for Wugongshan granites: (a) CJK06–2, (b) WGS06022, and (c) WGS06028.

For sample CJK06–2, 15 Hf isotopic analyses resulted in $\epsilon\text{Hf}(t)$ values of -9.34 to -6.19 and two-stage model (TDM2) ages of 1809–2006 Ma, with initial $^{176}\text{Hf}/^{177}\text{Hf}$ ratios of 0.282250–0.282337, and initial $^{176}\text{Lu}/^{177}\text{Hf}$ ratios varying from 0.000889 to 0.002222. There were 16 analyses of WGS06022, which produced $\epsilon\text{Hf}(t)$ values of -10.60 to -8.13 and TDM2 ages of 1930–2086 Ma, with initial $^{176}\text{Hf}/^{177}\text{Hf}$ ratios of 0.282219–0.282300, and $^{176}\text{Lu}/^{177}\text{Hf}$ ratios of 0.000715–0.002144. There were 18 analyses of WGS06028, which yielded $\epsilon\text{Hf}(t)$ values of -11.56 to -8.25 and TDM2 ages of 1940–2148 Ma, with initial $^{176}\text{Hf}/^{177}\text{Hf}$ ratios of 0.282202–0.282286, and $^{176}\text{Lu}/^{177}\text{Hf}$ ratios of 0.000934–0.002952 [54].

4.3. Geochemistry

Major- and trace-element compositions of 16 granites are listed in Supplementary Tables S2 and S3. The Wugongshan granite samples are characterized by 65.77–75.82 wt.% SiO_2 , 2.24–4.46 wt.% Na_2O , 2.64–4.95 wt.% K_2O , 0.08–1.40 wt.% MgO , 0.40–5.90 wt.% CaO , 12.16–15.46 wt.% Al_2O_3 and 0.02–0.59 wt.% TiO_2 , respectively. A total-alkali-silica (TAS) diagram shows that most samples plot in the granite fields (Figure 5a). Most have high $\text{K}_2\text{O}/\text{SiO}_2$ ratios and plot in the potassium field in the K_2O – SiO_2 diagram (Figure 5b). The samples are peraluminous, with A/CNK values of 0.68–1.31, ALK (total alkali ($\text{Na}_2\text{O} + \text{K}_2\text{O}$)) contents 5.18–8.62 wt.%, and A/NK values of 1.22–2.15 (Figure 5c). In the AFM diagram, the samples plot in the Calc-alkali field (Figure 5d).

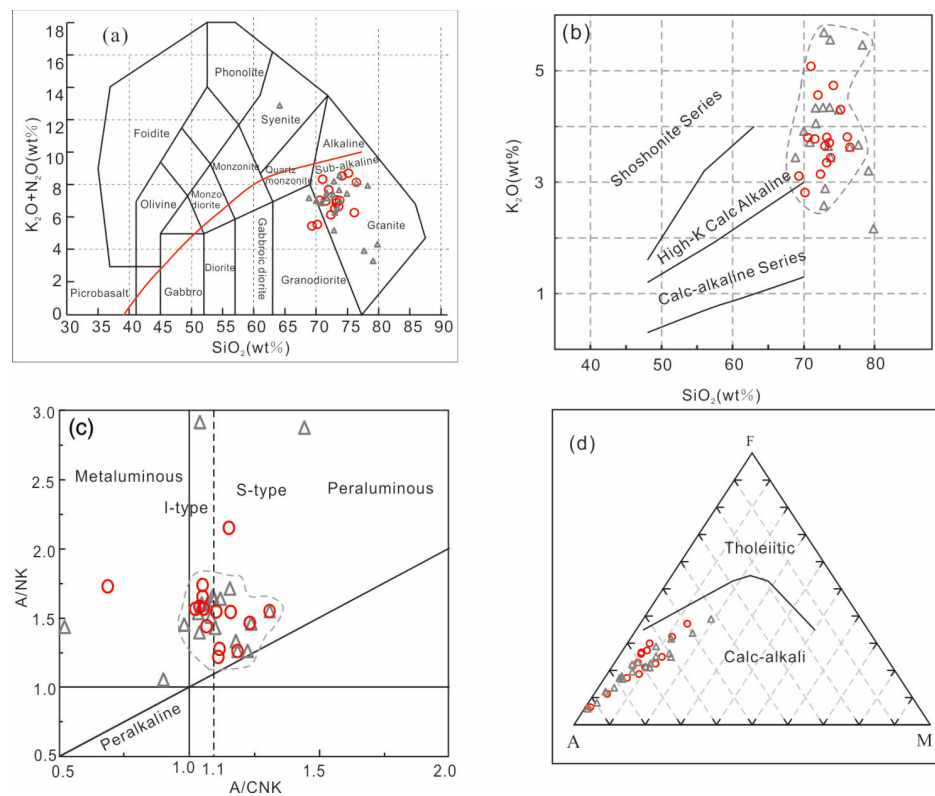


Figure 5. (a) Total-alkali-silica (TAS) diagram; (b) K_2O – SiO_2 diagram (after [55,56]); (c) the A/NK – A/CNK diagram (from [57]); and (d) AFM diagram (from [58,59]) for the Wugongshan granites. The triangle denotes published data for the Wugongshan granites ([24]; and reference data; the same below).

The Wugongshan Paleozoic granite samples are characterized by relatively uniform trace-element compositions. The granite samples have total rare earth element (ΣREE) contents of 13.29–334.05 ppm, and all granite samples show light REE (LREE) enrichment and heavy REE (HREE) depletion in the chondrite-normalized REE diagram (Figure 6a; Table S3). The granites show $(La/Yb)_N$ values greater than 7.91 (except for samples XQZK11–1 and WGS06027), and have strongly negative Eu anomalies ($Eu/Eu^* = 0.51$ – 1.00) (except for samples WGS06027). In the N-MORB-normalized spider diagram (Figure 6b), the Wugongshan granites exhibit positive K, U, and Pb anomalies and negative Ba, Nb, Ce, Sr, P, and Ti anomalies.

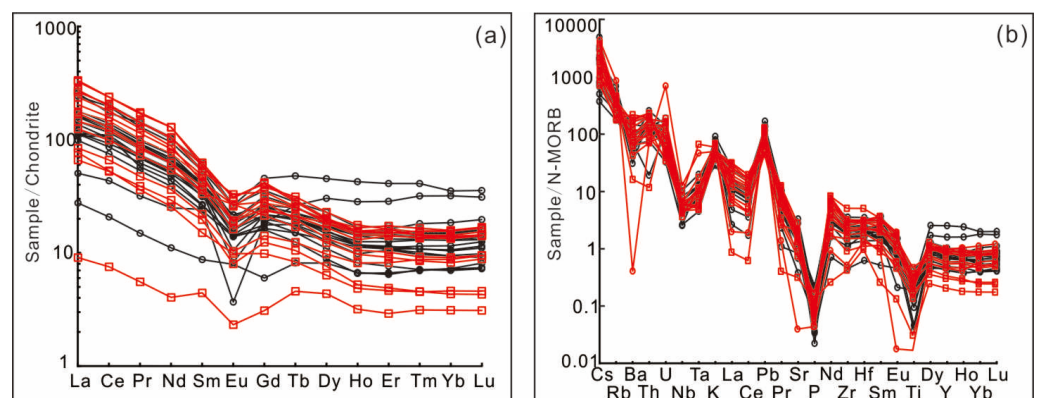


Figure 6. (a) Chondrite-normalized REE and (b) N-MORB-normalized spider patterns of the Wugongshan granites (normalizing factors are from [60,61]; N-MORB compositions are from [60]). The black lines indicate published data for the Wugongshan granites ([24]; and reference data).

5. Discussion

5.1. Ages

The age results of the representative Wugongshan granites show that the zircon U–Pb age is 438.9 ± 1.2 Ma– 441.2 ± 1.6 Ma, indicating that the Wugongshan granite was formed in the Early Silurian Period. The previous research results show that the Early Paleozoic granite age in the Wugongshan area is roughly concentrated in three periods: 455 Ma, 440 Ma, and 425 Ma and the granites under investigation represent the age range of the second periods (438–442 Ma), respectively.

Early Paleozoic igneous rocks were widespread in the SCC, with most having formed during the Caledonian stage (460–410 Ma) [14,17,19,24]. The classification of the Wugongshan granites in northwestern Jiangxi is still under discussion. The Wugongshan granites have peraluminous characteristics, as indicated by their A/NK ratios (1.22–2.15), and A/CNK ratios (0.68–1.31). In the A/NK–A/CNK diagram, all points are placed on the I–S granite boundary area (Figure 5c).

In summary, Wugongshan granites are S-type rather than I-type, as indicated by an A/CNK > 1.1 and widespread Al-rich minerals (e.g., muscovite), together with alkaline minerals (e.g., iron-rich biotite), which indicate that the Wugongshan granites belong to muscovite-bearing peraluminous granites (MPG) [62–69].

5.2. Nature of Sources

The Wugongshan granite's characteristics indicate that the magma is mainly formed by the partial melting of upper crust material, and there are no obvious mantle-source materials in the magma formation process. The δEu of Wugongshan granites is 0.51–1.00 (except WGS06027), indicating that plagioclase separation and crystallization occurred during the magmatic evolution, which mainly comes from the partial remelting of upper crustal materials [62,65,66]. The moderate negative δEu anomaly, a relatively flat distribution pattern of heavy rare earth elements (HREE), and negative Ba and Sr anomalies, may indicate that residual minerals in the source contain a certain amount of feldspar [62]. The zircons from different sources often have different Hf isotopic characteristics, so the magma source characteristics can be traced with the Hf isotopes [49,70–72]. The single-stage mode age (t_{DM}) of Wugongshan granite zircon Hf was 1305–1540 Ma, and the two-stage mode age ($t_{\text{DM}2}$) was 1809–2148 Ma. The $(\text{Lu}/\text{Hf})_f$ of Wugongshan granite is -0.98 – -0.91 , which is significantly lower than that of the continental crust (-0.72 , Vervoort et al., 1996). All the zircon $\epsilon\text{Hf}(t)$ is negative (-11.56 – -6.19), except for some points near the 1.8Ga trend evolution line. Other points are projected between the 1.8 Ga and 2.5 Ga trend evolution lines, indicating that the Wugongshan granites were derived from the partial melting of ancient crust and significant crustal reworking (Figure 7).

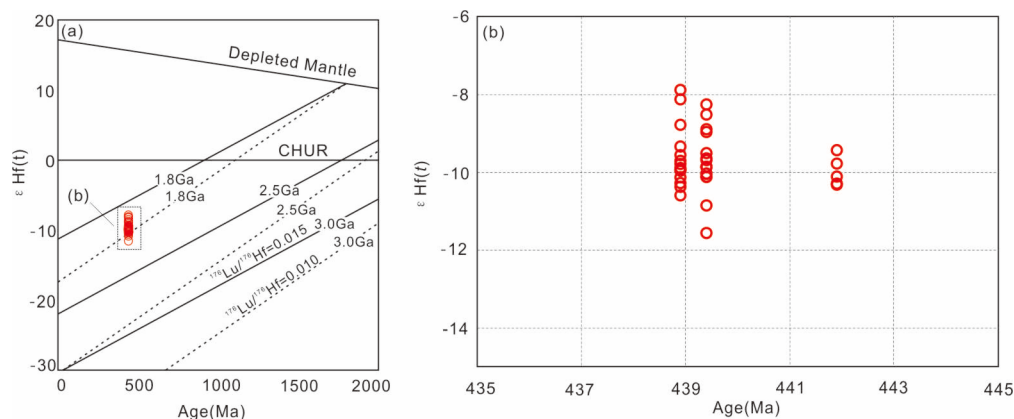


Figure 7. The data of zircon $\epsilon\text{Hf}(t)$ vs. $^{206}\text{Pb}/^{238}\text{U}$ ages for Wugongshan granites (a,b), indicating that the magma was formed by the reworking of the upper-middle crust. The corresponding lines are from [49].

The Wugongshan granites have relatively low Rb/Sr and Rb/Ba ratios, implying an affinity with pelite-derived and psammite-derived melt, and all samples plot in the clay-poor field in the Rb/Ba–Rb/Sr diagram (Figure 8a; [73]). In the CaO/Na₂O–Al₂O₃/TiO₂ diagram (Figure 8b), the Wugongshan granites display varied CaO/Na₂O ratios, and the spots plot in the pelite-derived field, indicating the magma was derived from partial melting of the pelite rocks from the Paleoproterozoic continental crust [73].

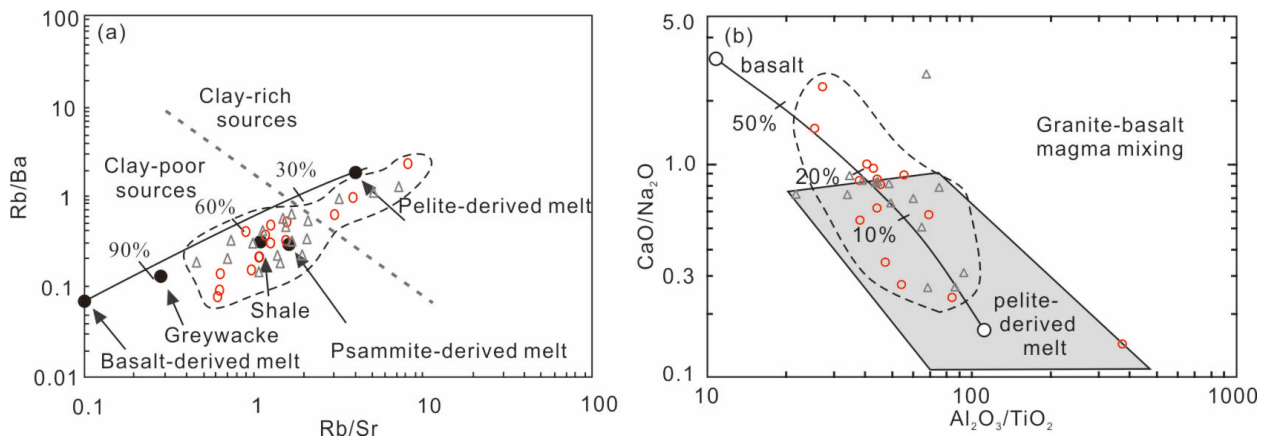


Figure 8. Rb/Ba–Rb/Sr (after [73]) (a) and CaO/Na₂O–Al₂O₃/TiO₂ (b) (from [73]) diagrams for the Wugongshan granites.

Recent studies have shown that the content and ratio of Sr and Y elements in granites are closely related to the residual facies in the magmatic source [74]. During the partial melting of magmatic rocks, Nb and Ta often remain in hornblende, while Ti remains in rutile [75]. The obvious loss of Sr, Ba, and Ti from the Wugongshan granite suggests that plagioclase and Ti-containing minerals (such as biotite) have undergone obvious separation and magma crystallization. When the content of garnet in the residual phase of the magma source reaches 10%, the magma has the characteristics of high Sr and low Y [76]. If the residual facies in the magma source are dominated by hornblende, Y/Yb is close to 10. If the residual facies in the magma source are dominated by garnet, the ratio is significantly greater than 10 [77]. The composition of the Wugongshan granites showed that the Y/Yb ratio was 7.15–12.65 and close to 10, and the rock mass did not have the characteristics of adakite (high Sr and low Y), indicating that the magma source was dominated by hornblende residues. The Wugongshan granites have δEu anomalies (0.51–1.00, except WGS06027), indicating that there are plagioclase residues in the magmatic source [65].

Based on the above discussion of the analysis, we infer that the residual facies of the Wugongshan granites in the magma source are amphibolite facies, and the residual mineral assemblage is hornblende + plagioclase.

5.3. Tectonic Implications

The tectonic setting of South China in the Early Paleozoic orogeny has been controversial. Some scholars have ascribed the Paleozoic orogeny to an oceanic subduction and collision setting, with the ocean basin situated between the Yangtze and Cathaysia blocks [25,26,78,79]. Others proposed that it was an intracontinental orogeny with no ocean basin separation between the two blocks [13,14,17,24,78,79]. As an important part of the continental crust, granites can be formed in different tectonic settings, such as active continental margins, continental crust-thickening stages of collision, and post-orogenic extensional tectonic settings [57,80,81]. There are no records of oceanic crust remnants or fragments along the boundary between the Yangtze and Cathaysia blocks in the Early Paleozoic period, and no ophiolite or arc-related magmatic rock development during that time [8,9,12,13,15,19]. The widely developed S-type granites and the absence of high-pressure, low-temperature metamorphism in the Caledonian orogenic belt in the SCC is

inconsistent with an oceanic subduction setting [13,17,78]. Therefore, it does not belong to the Andean-type orogeny formed by the subduction of the oceanic plate under the continental plate in the Caledonian orogenic belt in the SCC.

The Early Paleozoic magmatic rocks are widely distributed in the Yangtze and Cathaysia blocks and their ages were construed to be ca. 460–410 Ma, without developing along the subduction zone [13,17,78]. The palaeogeographic studies of South China show that there is a lack of active continental margin sedimentation, or similar sedimentary environment facies, along the boundary between the Yangtze and Cathaysia blocks [13,17,78]. The paleontological strata and paleoecological evolution between the Yangtze block and the Cathaysia block are related and continuous and belong to the unified continental basin's paleogeographical environment in the Early Paleozoic [13,17,78]. The Early Paleozoic–Caledonian orogeny in South China is an intracontinental orogenic event that developed from the Middle Ordovician (>460 Ma) to the Early Devonian (about 415 Ma), while the Wugongshan granite was formed in the intracontinental setting rather than the continental collision setting [14,23].

In the Hf–(Rb/10)–(3Ta) discrimination diagram (Figure 9a; [82]), the Wugongshan samples plot in the collisional granites field (COLG), while in the Hf–(Rb/30)–(3Ta) diagram (Figure 9b) the samples plot in the overlapping field of post-collisional granites (P-COLG) and syn-collisional granites (S-COLG). In the Rb–(Yb+Ta) diagram, Rb–(Y+Nb) diagram, Nb–Y diagram, and Ta–Yb diagram, all the samples plot in the overlapping field of S-COLG and volcanic arc granites (VAG) (Figure 10; [83]). Given the intracontinental orogenic characteristic, S-type granite, and relatively uniform negative Lu–Hf isotopic compositions, Wugongshan granites were formed in the process of the collision or post-collision extensional tectonic setting [23,24,80,82]. These studies of granulites from Yiyang, Yunkai, and Taoxi indicate that the rocks have a clockwise P–T–t path, and the zircon indicates that the time of subduction and exhumation was ca. 440 Ma [78]. The Early Paleozoic granites and the granulites in Wugongshan have the same U–Pb age, which indicates that the Wugongshan pluton developed in the post-collision extensional tectonic background [24,80].

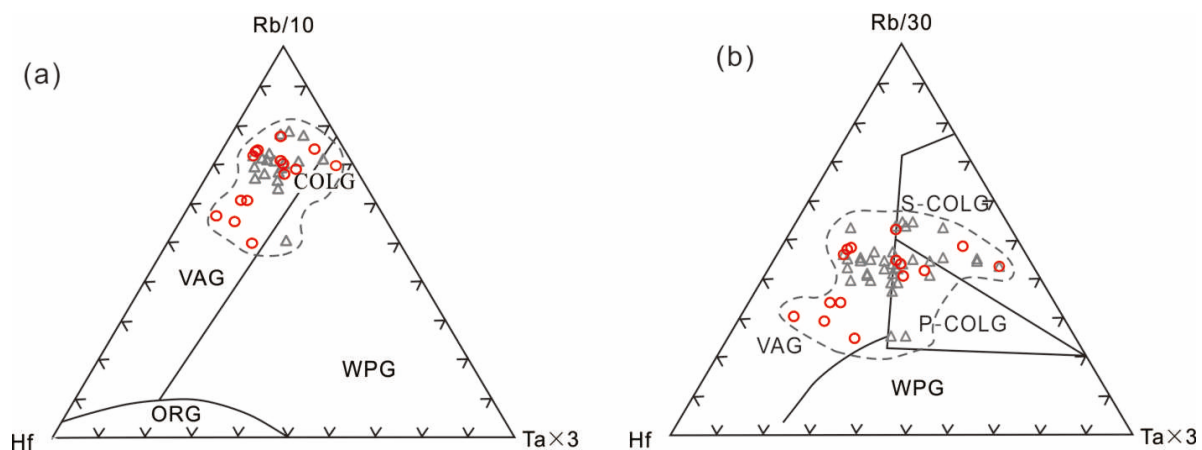


Figure 9. Tectonic discrimination diagrams for Wugongshan granites. (a) Rb/10–Hf–(3Ta); (b) Rb/30–Hf–(3Ta) (after [82]). COLG—collisional granite; VAG—volcanic arc granite; WPG—within-plate granite; S-COLG—syn-collisional granite; ORG—oceanic ridge granite; P-COLG—post-collisional granite.

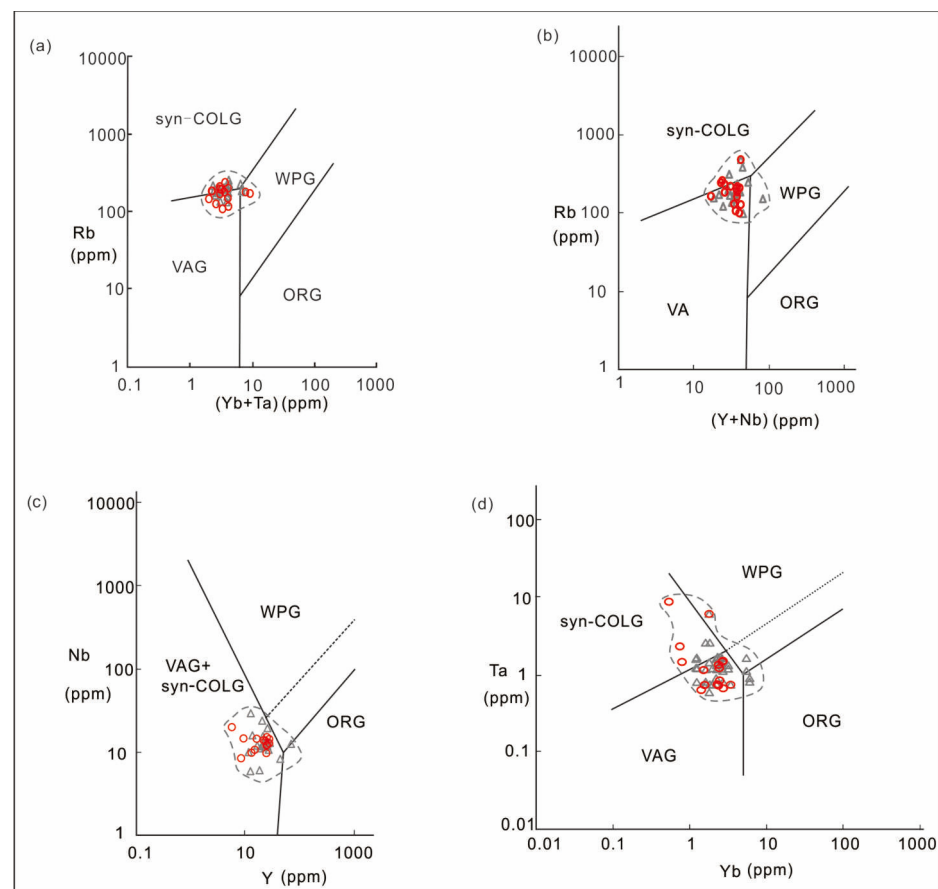


Figure 10. Tectonic discrimination diagrams for Wugongshan granites: (a) Rb–(Yb+Ta) diagrams; (b) Rb–(Y+Nb) diagrams; (c) Nb–Y diagrams; (d) Ta–Yb diagrams (from [83]).

With the continental collision of the Yangtze block and Cathaysia block, the Paleo-Tethys Ocean closed along the Jiangshan-Shaoxing fault zone during the Neoproterozoic (ca. 850–820 Ma) (Figure 1b) [14,28]. The later bimodal magmatism, diabasic dykes, and the depression basin, probably represent the Neoproterozoic rifting (ca. 840–760 Ma) (Figure 11a) [14,28]. From the Ediacaran to the Early Paleozoic (760–460 Ma), the SCC sediments were deposited in a stable neritic-slope environment, which was not obviously affected by the Pan-African movement (Figure 11b) [13,17,28,78]. From the late Ordovician (ca. 460 Ma), the intracontinental granitic magmatism widespread in the SCC was the tectonic response to the closure of the Proto-Tethys Ocean (Figure 11) [14,24,78]. Finally, magma intrusion occurred during the post-orogenic stage, which is consistent with the occurrence of the Wugongshan granitic intrusions (Figure 11). Here, we invoke a model similar to that proposed by [28] and [14] to account for the tectonic evolution of the SCC (Figure 11).

Considering that the Indochina block in Vietnam’s subduction north to south China occurred along with the subduction of the Proto-Tethys Ocean during the Paleozoic [16,17], given the combined effects of oceanic–continental subduction the intracontinental subduction of the Yangtze block and Cathaysia block resulted in the superposition of two continental crust slabs and the thickening of the continental crust (Figure 11c). Thereafter, the Wugongshan granites intruded under the intracontinental tectonic plates in response to the distant stresses of the convergence of the Proto-Tethys Ocean.

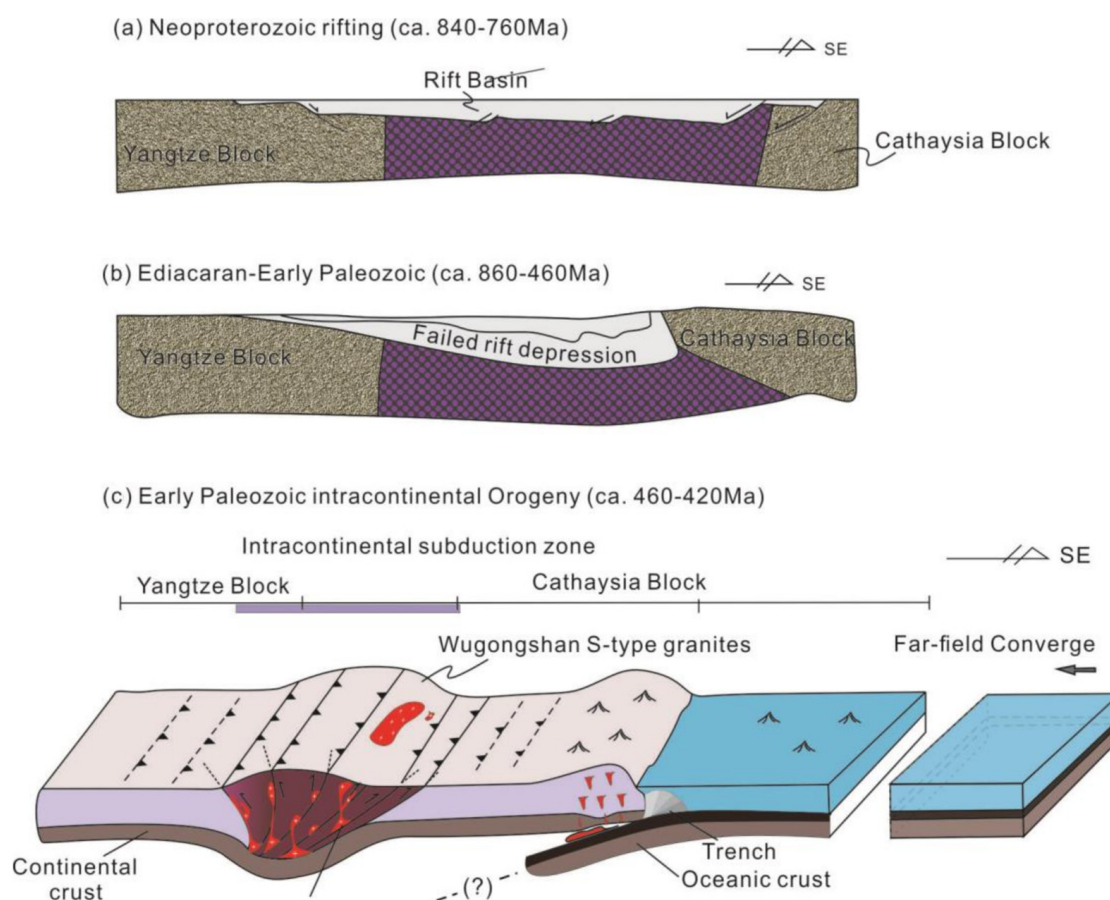


Figure 11. The dynamic model of the Neoproterozoic to the Paleozoic tectonic evolution of South China (non-scale for crust and lithosphere) (modified from [14,28,62]).

6. Conclusions

- (1) The U–Pb ages of the granites indicated that the Wugongshan granites were emplaced in 442–438 Ma.
- (2) Their strongly peraluminous nature, combined with the presence of muscovite, indicates that Wugongshan granites are S–type granites. The Hf isotopic compositions and the geochemical characteristics of the Wugongshan granites indicate that the magmas were derived from partial melting of the upper crust of the SCC.
- (3) The Caledonian granites in the Wugongshan area are being generated in an intracontinental orogenic setting, which is a far–field effects response to the convergence of the Paleo-Tethys Ocean.

Supplementary Materials: The following supporting information can be downloaded at: <https://www.mdpi.com/article/10.3390/min13111427/s1>, Supplementary Table S1. LA–ICP–MS U–Pb zircon ages of Wugongshan granite samples CJK06–2, WGS06022, and WGS06022; Supplementary Table S2. Whole-rock major–oxide (wt.%) compositions of the Wugongshan granites; Supplementary Table S3. Whole-rock trace–element (ppm) compositions of the Wugongshan granites; Supplementary Table S4. Zircon Hf isotopic compositions of the Wugongshan granites.

Author Contributions: Conceptualization, G.Y., Y.Z. (Yaoyao Zhang) and H.H.; methodology, G.Y.; software, H.H.; validation, K.L. and Y.Z. (Yi Zhou); formal analysis, G.Y.; investigation, G.Y., Y.Z. (Yi Zhou) and H.H.; resources, G.Y. and S.W.; data curation, H.H. and G.Y.; writing—original draft preparation, G.Y.; writing—review and editing, Y.Z. (Yi Zhou) and G.Y.; visualization, G.Y.; supervision, G.Y. and Y.Z. (Yi Zhou); project administration, Y.Z. (Yi Zhou); funding acquisition, G.Y. and H.H. All authors have read and agreed to the published version of the manuscript.

Funding: This study was supported by the fundamental research funds of CGS Research (JKYQN202307), the National Natural Science Foundation of China (grant Nos. U2244205), the Joint Innovation Fund of China National Uranium Co., Ltd. and State Key Laboratory of Nuclear Resources and Environment (No. NRE2021-01), and the China Geological Survey Bureau (DD20221677-2).

Data Availability Statement: Not applicable.

Acknowledgments: The authors thank Qiuye Yu of the Changchun Institute of Technology and Lele Han of China University of Geosciences (Beijing) for the computer mapping work.

Conflicts of Interest: The authors declare no conflict of interest.

References

1. Charvet, J.; Shu, L.S.; Shi, Y.S.; Guo, L.Z.; Faure, M. The building of south China: Collision of Yangtze and Cathaysia blocks, problems and tentative answers. *J. Southeast Asian Earth Sci.* **1996**, *13*, 223–235. [[CrossRef](#)]
2. Charvet, J.; Shu, L.S.; Faure, M.; Choulet, F.; Wang, B.; Lu, H.F.; Breton, N.L. Structural development of the lower Paleozoic belt of South China: Genesis of an intracontinental orogen. *J. Asian Earth Sci.* **2010**, *39*, 309–330. [[CrossRef](#)]
3. Faure, M.; Sun, Y.; Shu, L.Y.; Monie, P.; Charvet, J. Extensional tectonics within a subduction-type orogen. The case study of the Wugongshan dome (Jiangxi Province, southeastern China). *Tectonophysics* **1996**, *263*, 77–106. [[CrossRef](#)]
4. Faure, M.; Der, A.W.; Walt, V.A. *Globalization and Private Law: The Way Forward*; Edward Elgar: Cheltenham, UK, 2010.
5. Hsü, K.J.; Li, J.; Chen, H.; Wang, Q.; Sun, S.; Şengör, A.M.C. Tectonics of South China: Key to understanding West Pacific geology. *Tectonophysics* **1990**, *183*, 9–39. [[CrossRef](#)]
6. Li, Z.X. Tectonic history of the major East Asian lithospheric blocks since the mid-Proterozoic—A synthesis. In *Mantle Dynamics and Plate Interactions in East Asia*; Geodynamics Series; American Geophysical Union: Washington, DC, USA, 1998; Volume 27, pp. 221–243.
7. Li, W.X.; Li, X.H.; Li, Z.X.; Lou, F.S. Obduction-type granites within the NE Jiangxi Ophiolite: Implications for the final amalgamation between the Yangtze and Cathaysia Blocks. *Gondwana Res.* **2008**, *13*, 288–301. [[CrossRef](#)]
8. Li, X.H.; Li, W.X.; Li, Z.X.; Liu, Y. 850–790 Ma bimodal volcanic and intrusive rocks in northern Zhejiang, South China: A major episode of continental rift magmatism during the breakup of Rodinia. *Lithos* **2008**, *102*, 341–357. [[CrossRef](#)]
9. Li, X.H.; Li, W.X.; Li, Z.X.; Lo, C.H.; Wang, J.; Ye, M.F.; Yang, Y.H. Amalgamation between the Yangtze and Cathaysia Blocks in South China: Constraints from SHRIMP U–Pb zircon ages, geochemistry and Nd–Hf isotopes of the Shuangxiwu volcanic rocks. *Precambrian Res.* **2009**, *174*, 117–128. [[CrossRef](#)]
10. Lin, S.F.; Xing, G.F.; Davis, D.W.; Yin, C.Q.; Wu, M.L.; Li, L.M.; Jiang, Y.; Chen, Z.H. Appalachian-style multi-terrane Wilson cycle model for the assembly of South China. *Geology* **2018**, *46*, 319–322. [[CrossRef](#)]
11. Wang, X.L.; Zhou, J.C.; Qiu, J.S.; Gao, J.F. Geochemistry of the Meso- to Neoproterozoic basic–acid rocks from Hunan Province, South China: Implications for the evolution of the western Jiangnan orogen. *Precambrian Res.* **2004**, *135*, 79–103. [[CrossRef](#)]
12. Wang, X.L.; Zhou, J.C.; Griffin, W.L.; Wang, R.C.; Qiu, J.S.; Reilly, S.Y.; Xu, X.; Liu, X.M.; Zhang, G.L. Detrital zircon geochronology of Precambrian basement sequences in the Jiangnan orogen: Dating the assembly of the Yangtze and Cathaysia Blocks. *Precambrian Res.* **2007**, *159*, 117–131. [[CrossRef](#)]
13. Li, Z.X.; Li, X.H. Formation of the 1300-km-wide intracontinental orogen and postorogenic magmatic province in Mesozoic South China: A flat-slab subduction model. *Geology* **2007**, *35*, 179–182. [[CrossRef](#)]
14. Li, Z.X.; Li, X.H.; Wartho, J.A.; Clark, C.; Li, W.X.; Zhang, C.L.; Bao, C.M. Magmatic and metamorphic events during the Early Paleozoic Wuyi Yunkai orogeny, southeastern South China: New age constraints and pressure–temperature conditions. *Geol. Soc. Am. Bull.* **2010**, *122*, 772–793. [[CrossRef](#)]
15. Li, S.Z.; Santosh, M.; Zhao, G.C.; Zhang, G.W.; Jin, C. Intracontinental deformation in a frontier of super-convergence: A perspective on the tectonic milieu of the South China Block. *J. Asian Earth Sci.* **2012**, *49*, 313–329. [[CrossRef](#)]
16. Wang, Y.J.; Fan, W.M.; Zhao, G.C.; Ji, S.C.; Peng, T.P. Zircon U–Pb geochronology of gneissic rocks in the Yunkai massif and its implications on the Caledonian event in the South China block. *Gondwanan Res.* **2007**, *12*, 404–416. [[CrossRef](#)]
17. Wang, Y.J.; Zhang, F.F.; Fan, W.M.; Zhang, G.W.; Chen, S.Y.; Cawood, P.A.; Zhang, A.M. Tectonic setting of the South China Block in the Early Paleozoic: Resolving intracontinental and ocean closure models from detrital zircon U–Pb geochronology. *Tectonics* **2010**, *29*, 6020–6035. [[CrossRef](#)]
18. Li, J.L. Tectonic framework and evolution of southeastern China. *J. Southeast Asian Earth Sci.* **1993**, *8*, 219–223.
19. Wang, Y.; Zhang, A.; Fan, W.; Zhao, G.; Zhang, G.; Zhang, Y.; Zhang, F.; Li, S. Kwanghsian crustal anatexis within the eastern South China Block: Geochemical, Zircon U–Pb geochronological and Hf isotopic fingerprints from the gneissoid granites of Wugong and Wuyi–Yunkai Domains. *Lithos* **2011**, *127*, 239–260. [[CrossRef](#)]
20. Wang, D.; Zheng, J.P.; Ma, Q.; Griffin, W.L.; Zhao, H.; Wong, J. Early Paleozoic crustal anatexis in the intraplate Wuyi–Yunkai orogen, South China. *Lithos* **2013**, *175–176*, 124–145. [[CrossRef](#)]
21. Zhang, G.W.; Guo, A.L.; Wang, Y.J.; Li, S.Z.; Dong, Y.P.; Liu, S.F.; He, D.F.; Cheng, S.Y.; Lu, R.K.; Yao, A.P. Tectonics of South China continent and its implications. *Sci. China Earth Sci.* **2013**, *56*, 1804–1828. (In Chinese with English Abstract) [[CrossRef](#)]
22. Zhao, G.C.; Guo, J.H. Precambrian geology of China: Preface. *Precambrian Res.* **2012**, *222–223*, 1–12. [[CrossRef](#)]

23. Yao, W.H.; Li, Z.X.; Li, W.X.; Wang, X.C.; Li, X.H.; Yang, J.H. Post-kinematic lithospheric delamination of the Wuyi–Yunkai orogen in South China: Evidence from ca. 435Ma high–Mg basalts. *Lithos* **2012**, *154*, 115–129. [[CrossRef](#)]
24. Zhang, Y.Y.; Liu, K.; He, Q.C.; Tong, Y.; Deng, Y.F.; Yu, C.H.; Sun, J.L.; Yu, T.X.; Guo, J.H.; Wang, S.X. Petrological, zircon U–Pb, Lu–Hf isotopic geochemical characteristics of the Early Paleozoic granites in Wugong Mountain area, Jiangxi Province, and their geological significance. *Geol. Rev.* **2022**, *69*, 1004–1020. (In Chinese with English Abstract)
25. Peng, S.B.; Liu, S.F.; Lin, M.S.; Wu, C.F.; Han, Q.S. Early Paleozoic Subduction in Cathaysia (I): New Evidence from Nuodong Ophiolite. *Earth Sci.* **2016**, *41*, 765–778. (In Chinese with English Abstract)
26. Peng, S.B.; Liu, S.F.; Lin, M.S.; Wu, C.F.; Han, Q.S. Early Paleozoic Subduction in Cathaysia (II): New Evidence from the Dashuang High Magnesian–Magnesian Andesite. *Earth Sci.* **2016**, *41*, 931–947. (In Chinese with English Abstract)
27. Shu, L.S.; Song, M.J.; Yao, Y.L. Appalachian-style multi-terrane Wilson cycle model for the assembly of South China: COMMENT. *Geology* **2018**, *46*, e445. [[CrossRef](#)]
28. Shu, L.S.; Yao, J.L.; Wang, B.; Faure, M.; Charvet, C.; Chen, Y. Neoproterozoic plate tectonic process and Phanerozoic geodynamic evolution of the South China Block. *Earth–Sci. Rev.* **2021**, *216*, 103596. [[CrossRef](#)]
29. Faure, M.; Charvet, J.; Chen, Y. Appalachian-style multi-terrane Wilson cycle model for the assembly of South China: COMMENT. *Geology* **2018**, *46*, e446. [[CrossRef](#)]
30. Guo, L.Z.; Shi, Y.S.; Lu, H.F.; Ma, R.S.; Dong, H.G.; Yang, S.F. The Pre-devonian tectonic patterns and evolution of South China. *J. Asian Earth Sci.* **1989**, *3*, 87–93.
31. Li, J.H.; Dong, S.W.; Cawood, P.A.; Zhao, G.C.; Johnston, S.T.; Zhang, Y.Q.; Xin, Y.J. An Andean-type retro-arc foreland system beneath northwest South China revealed by SINOPROBE profiling. *Earth Planet. Sci. Lett.* **2018**, *490*, 170–179. [[CrossRef](#)]
32. Faure, M.; Shu, L.S.; Wang, B.; Charvet, J.; Choulet, F.; Monie, P. Intracontinental subduction: A possible mechanism for the Early Palaeozoic Orogen of SE China. *Terra Nova* **2009**, *21*, 360–368. [[CrossRef](#)]
33. Zhang, F.R. The character and emplacement mechanism of gneiss in Wugong Mountain. *J. East China Geol. Inst.* **2000**, *23*, 146–149. (In Chinese with English Abstract)
34. Lou, F.; Shen, W.; Wang, D.; Shu, L.; Wu, F.; Zhang, F.; Yu, J. Zircon U–Pb isotopic chronology of the Wugongshan dome compound granite in Jiangxi Province. *Acta Geol. Sin.* **2005**, *79*, 636–644.
35. Sun, Y.; Shu, L.; Faure, M.; Charvet, J. Tectonic development of the metamorphic core complex of the Wugongshan in the northern Jiangxi Province. *J. Nanjing Univ. (Nat. Sci.)* **1997**, *33*, 447–449. (In Chinese with English Abstract)
36. Yu, Y.; Huang, X.L.; He, P.L.; Li, J. I-type granitoids associated with the Early Paleozoic intracontinental orogenic collapse along pre-existing block boundary in South China. *Lithos* **2016**, *248–252*, 353–365. [[CrossRef](#)]
37. Zhang, F.R.; Shu, L.S.; Wang, D.Z.; Yu, J.H.; Shen, W.Z. Discussions on the tectonic setting of Caledonian granitoids in the eastern segment of South China. *Earth Sci. Front.* **2009**, *16*, 248–260. (In Chinese with English Abstract)
38. Zhang, F.F.; Wang, Y.J.; Fan, W.M.; Zhang, A.M.; Zhang, Y.Z. LA–ICPMS zircon U–Pb geochronology of late Early Paleozoic granites in eastern Hunan and western Jiangxi provinces, South China. *Geochimica* **2010**, *39*, 414–426. (In Chinese with English Abstract)
39. Zhang, F.F.; Wang, Y.J.; Fan, W.M.; Zhang, A.M.; Zhang, Y.Z. Zircon U–Pb Geochronology and Hf isotopes of the Neoproterozoic Granites in the Central of Jiangnan Uplift. *Geotecton. Metallog.* **2011**, *35*, 73–84. (In Chinese with English Abstract)
40. Zhang, F.F.; Wang, Y.J.; Zhang, A.M.; Fan, W.M.; Zhang, Y.Z.; Zi, J.W. Geochronological and geochemical constraints on the petrogenesis of Middle Paleozoic (Kwanghsian) massive granites in the eastern South China Block. *Lithos* **2012**, *150*, 188–208. [[CrossRef](#)]
41. Zhang, Y.Y.; Liu, K.; He, Q.C.; Hao, M.Y.; Guo, C.B.; Bai, J.J.; Yu, T.X. Zircon U–Pb ages, Hf isotopic characteristics, and geological significance of the Mesozoic granites in Wugong Mountains area, Jiangxi. *Geol. Rev.* **2022**, *68*, 1301–1319. (In Chinese with English Abstract)
42. Kwon, S.; Park, Y.; Park, C.; Kim, H.S. Mass-balance analysis of bulk-rock chemical changes during mylonitization of a megacryst-bearing granitoid, Cheongsan shear zone, Korea. *J. Asian Earth Sci.* **2009**, *35*, 489–501. [[CrossRef](#)]
43. Sun, S.S.; Dong, Y.P. High temperature ductile deformation, lithological and geochemical differentiation along the Shagou shear zone, Qinling Orogen, China. *J. Struct. Geol.* **2023**, *167*, 104791. [[CrossRef](#)]
44. Andersen, T. Correction of common lead in U–Pb analyses that do not report ²⁰⁴Pb. *Chem. Geol.* **2002**, *192*, 59–79. [[CrossRef](#)]
45. Goolaerts, A.; Mattielli, N.; Jong, J.D.; Weis, D.; Scoates, J.S. Hf and Lu isotopic reference values for the zircon standard 91500 by MC–ICP–MS. *Chem. Geol.* **2004**, *206*, 1–9. [[CrossRef](#)]
46. Ludwig, K.R. *User’s Manual for Isoplot 3.00: A Geochronological Toolkit for Microsoft Excel*; Berkeley Geochronology Center; Special Publication; No. 4; Berkeley Geochronology Center: Berkeley, CA, USA, 2003.
47. Hou, K.J.; Li, Y.H.; Tian, Y.R. In situ U–Pb zircon dating using laser ablation–multi ion counting–ICP–MS. *Miner. Depos.* **2009**, *28*, 481–492.
48. Griffin, W.L.; Pearson, N.J.; Belousova, E.; Jackson, S.E.; van Acherbergh, E.; O’Reilly, S.Y.; Shee, S.R. The Hf isotope composition of cratonic mantle: LAM–MC–ICPMS analysis of zircon megacrysts in kimberlites. *Geochim. Cosmochim. Acta* **2000**, *64*, 133–147. [[CrossRef](#)]
49. Griffin, W.L.; Wang, X.; Jackson, S.E.; Pearson, N.J.; Reilly, S.Y.; Xu, X.S.; Zhou, X.M. Zircon chemistry and magma mixing, SE China: In-situ analysis of Hf isotopes, Tonglu and Pingtan igneous complexes. *Lithos* **2002**, *61*, 237–269. [[CrossRef](#)]

50. Sláma, J.; Koler, J.; Condon, D.J.; Crowley, J.L.; Gerdes, A.; Hanchar, J.M.; Horstwood, M.S.; Morris, G.A.; Nasdala, L.; Norberg, N. Plešovice zircon—A new natural reference material for U–Pb and Hf isotopic microanalysis. *Chem. Geol.* **2008**, *249*, 1–35. [[CrossRef](#)]
51. Li, X.H. Geochemistry of the Longsheng Ophiolite from the southern margin of Yangtze Craton, SE China. *Geochem. J.* **1997**, *31*, 323–337. [[CrossRef](#)]
52. Belousova, E.A.; Griffin, W.L.; O'Reilly, S.Y.; Fisher, N. Igneous zircon: Trace element composition as an indicator of source rock type. *Contrib. Mineral. Petrol.* **2002**, *143*, 602–622. [[CrossRef](#)]
53. Rubatto, D.; Gebauer, D. Use of Cathodoluminescence for U–Pb Zircon Dating by Ion Microprobe: Some Examples from the Western Alps. In *Cathodoluminescence in Geosciences*; Springer: Berlin/Heidelberg, Germany, 2010. [[CrossRef](#)]
54. Stacey, J.S.; Kramers, J.D. Approximation of terrestrial lead isotope evolution by a two–stage model. *Earth Planet. Sci. Lett.* **1975**, *26*, 207–221. [[CrossRef](#)]
55. Peccerillo, A.; Taylor, S.R. Geochemistry of Eocene Calc Alkaline Volcanic Rocks from Kastamonu Area, Northern Turkey. *Contrib. Mineral. Petrol.* **1976**, *58*, 63–81. [[CrossRef](#)]
56. Le Bas, M.J.; Le Maitre, R.W.; Streckeisen, A.; Zanettin, B. A Chemical Classification of Volcanic Rocks Based on the Total Alkali–Silica Diagram. *J. Petrol.* **1986**, *27*, 745–750. [[CrossRef](#)]
57. Maniar, P.D.; Piccoli, P.M. Tectonic discrimination of granitoids. *Geol. Soc. Am. Bull.* **1989**, *101*, 635–643. [[CrossRef](#)]
58. Rickwood, O.C. Boundary lines within petrologic diagrams which use oxides of major and minor elements. *Lithos* **1989**, *22*, 247–263. [[CrossRef](#)]
59. Irvine, T.N.; Baragar, W.R.A. A guide to the chemical classification of the common volcanic rocks. *Can. J. Earth Sci.* **1971**, *8*, 523–548. [[CrossRef](#)]
60. Sun, S.S.; McDonough, W.F. Chemical and isotopic systematics of oceanic basalts: Implications for mantle composition and processes. In *Magmatism in the Ocean Basin*; Geological Society Special Publication: London, UK, 1989; Volume 42, pp. 313–345.
61. Boynton, W.V. Cosmochemistry of the Rare Earth Elements: Meteorite Studies. In *Rare Earth Element Geochemistry*; Henderson, P., Ed.; Elsevier: Amsterdam, The Netherlands, 1984; pp. 63–114.
62. Barbarin, B. A review of the relationships between granitoid types, their origins and their geodynamic environments. *Lithos* **1999**, *46*, 605–626. [[CrossRef](#)]
63. Deng, J.F.; Zhao, H.L.; Lai, S.C.; Luo, Z.H. Muscovite/two–mica granite and intracontinental subduction. *Earth Sci.* **1994**, *19*, 139–147. (In Chinese with English Abstract)
64. Deng, J.F.; Zhao, H.L.; Mo, X.X.; Liu, H.X.; Luo, Z.H. Intracontinental subduction of the Yangtze Continent and Continent reducing–inferred from muscovite (two mica) granites. *Geol. J. China Univ.* **1995**, *1*, 50–57. (In Chinese with English Abstract)
65. Middlemost, E.A.K. *Magma and Magmatic Rocks*; Longman: London, UK, 1985; pp. 1–266.
66. Middlemost, E.A.K. Naming materials in the magma/igneous rock system. *Earth–Sci. Rev.* **1994**, *37*, 215–224. [[CrossRef](#)]
67. Streckeisen, A. To each plutonic rock its proper name. *Earth–Sci. Rev.* **1976**, *12*, 1–33. [[CrossRef](#)]
68. Scaillet, B.; Holtz, F.; Pichavant, M. Experimental Constraints on the Formation of Silicic Magmas. *Elements* **2016**, *12*, 109–114. [[CrossRef](#)]
69. Vervoort, J.D.; Pachel, P.J.; Gehrels, G.E.; Nutman, A.P. Constraints on early Earth differentiation from hafnium and neodymium isotopes. *Nature* **1996**, *379*, 624–627. [[CrossRef](#)]
70. Amelin, Y.; Lee, D.C.; Halliday, A.N. Early–middle Archean crustal evolution deduced from Lu–Hf and U–Pb isotopic studies of single zircon grains. *Geochim. Cosmo Chim. Acta* **2000**, *64*, 4205–4225. [[CrossRef](#)]
71. Kinny, P.D.; Maas, R. Lu–Hf and Sm–Nd isotope systems in zircon. *Zircon. Rev. Mineral. Geochem.* **2003**, *53*, 327–341. [[CrossRef](#)]
72. Wu, F.Y.; Li, X.H.; Zheng, Y.F.; Gao, S. Lu–Hf isotopic systematics and their applications in petrology. *Acta Petrol. Sin.* **2007**, *23*, 185–220.
73. Sylvester, P.J. Post–collisional strongly peraluminous granites. *Lithos* **1998**, *45*, 29–44. [[CrossRef](#)]
74. Defant, M.J.; Drummond, M.S. Derivation of some morden arc magmas by of young subducted lithosphere. *Nature* **1990**, *347*, 662–665. [[CrossRef](#)]
75. Rollison, H.R. *Using Geochemical Data: Evaluation, Presentation, Interpretation*; Longman Group UK Ltd.: London, UK, 1993; pp. 107–135.
76. Hollocher, B.J.; Robinson, P. Geochemistry of the metamorphosed Ordovician Taconian Magmatic Arc, Bronson Hill anticlinorium, western New England. *Phys. Chem. Earth* **2002**, *27*, 5–45. [[CrossRef](#)]
77. Ge, X.Y.; Li, X.H.; Chen, Z.G.; Li, W.P. Geochemical characteristics and genesis of Yanshanian high Sr and low Y type intermediate–acid volcanic rocks in eastern China: Constraints on crustal thickness in eastern China. *Chin. Sci. Bull.* **2002**, *47*, 474–480. (In Chinese with English Abstract)
78. Yu, J.H.; Lou, F.S.; Wang, L.J.; Shen, L.W.; Zhou, X.Y.; Zhang, C.H.; Huang, Z.Z. The geological significance of a Paleozoic mafic granulite found in the Yiyang area of northeastern Jiangxi Province. *Chin. Sci. Bull. (Chin. Ver.)* **2014**, *59*, 3508–3516. (In Chinese with English Abstract) [[CrossRef](#)]
79. Zhong, Y.F.; Wang, L.X.; Zhao, J.H.; Liu, L.; Ma, C.Q.; Zheng, J.P.; Zhang, Z.; Luo, B.J. Partial melting of an ancient sub–continental lithospheric mantle in the Early Paleozoic intracontinental regime and its contribution to petrogenesis of the coeval peraluminous granites in South China. *Lithos* **2016**, *264*, 224–238. [[CrossRef](#)]
80. Deng, J.F.; Feng, Y.F.; Di, Y.J.; Liu, C.; Xiao, Q.H.; Su, S.G.; Zhao, G.C.; Meng, F.; Xiong, L. The intrusive spatial temporal evolutionary framework in the Southeast China. *Geol. Rev.* **2016**, *62*, 3–16. (In Chinese with English Abstract)

81. Martínez, E.M.; Villaseca, C.; Orejana, D.; Pérez-Soba, C.; Belousova, E.; Andersen, T. Tracing magma sources of three different S-type peraluminous granitoid series by in situ U–Pb geochronology and Hf isotope zircon composition: The Variscan Montes de Toledo batholith (central Spain). *Lithos* **2014**, *200–201*, 273–298. [[CrossRef](#)]
82. Harris, N.B.W.; Pearce, J.A.; Tindle, A.G. Geochemical characteristics of collision-zone magmatism. In *Geological Society; Special Publications*: London, UK, 1986; Volume 19, pp. 67–81.
83. Pearce, J.A.; Harris, N.B.W.; Tindle, A.G. Trace element discrimination diagrams for the tectonic interpretation of granitic rocks. *J. Petrol.* **1984**, *25*, 956–983. [[CrossRef](#)]

Disclaimer/Publisher’s Note: The statements, opinions and data contained in all publications are solely those of the individual author(s) and contributor(s) and not of MDPI and/or the editor(s). MDPI and/or the editor(s) disclaim responsibility for any injury to people or property resulting from any ideas, methods, instructions or products referred to in the content.